Journal of Solid State Chemistry 242 (2016) 96–101

Contents lists available at ScienceDirect

Journal of Solid State Chemistry

journal homepage: www.elsevier.com/locate/jssc

# $Cr_2O_5$ as new cathode for rechargeable sodium ion batteries

Xu-Yong Feng [a], Po-Hsiu Chien [a], Alyssa M. Rose [a], Jin Zheng [a], Ivan Hung [b], Zhehong Gan [b], Yan-Yan Hu [a,b,*]

[a] Department of Chemistry and Biochemistry, Florida State University, Tallahassee, FL 32306, USA
[b] Centre of Interdisciplinary Magnetic Resonance, National High Magnetic Field Laboratory, 1800 East Paul Dirac Drive, Tallahassee, FL 32310, USA

ARTICLE INFO

*Article history:*
Received 27 February 2016
Received in revised form
22 April 2016
Accepted 2 May 2016
Available online 3 May 2016

*Keywords:*
Chromium oxides
Sodium ion batteries
Solid-state $^{23}$Na NMR
High-valent transition metal

ABSTRACT

Chromium oxide, $Cr_2O_5$, was synthesized by pyrolyzing $CrO_3$ at 350 °C and employed as a new cathode in rechargeable sodium ion batteries. $Cr_2O_5$/Na rechargeable batteries delivered high specific capacities up to 310 mAh/g at a current density of C/16 (or 20 mA/g). High-resolution solid-state $^{23}$Na NMR both qualitatively and quantitatively revealed the reversible intercalation of Na ions into the bulk electrode and participation of Na ions in the formation of the solid-electrolyte interphase largely at low potentials. Amorphization of the electrode structure occurred during the first discharge revealed by both NMR and X-ray diffraction data. $CrO_3$-catalyzed electrolyte degradation and loss in electronic conductivity led to gradual capacity fading. The specific capacity stabilized at $>$ 120 mAh/g after 50 charge-discharge cycles. Further improvement in electrochemical performance is possible via electrode surface modification, polymer binder incorporation, or designs of new morphologies.



## 1. Introduction

The development of low-cost and safe rechargeable batteries with high energy and power densities is one of the major pursuits in furthering energy storage technologies. The wider-spread availability and much lower cost of sodium compared with lithium have attracted tremendous attention to rechargeable sodium ion batteries [1–3]. The similarities in chemical and physical properties that Na and Li bear mean that some electrode materials previously developed for lithium ion batteries can be readily adapted to sodium ion batteries. For instance, anodes include carbon (hard carbon) based materials [4,5], alloys (Si and Sn) [6,7], and $Li_4Ti_5O_{12}$ [8,9], and cathodes include layer-structured materials ($NaCrO_2$, $NaFeO_2$, and $Na_xCo_{1/3}Ni_{1/3}Mn_{1/3}O_2$ [10–12]) and Na Super Ionic Conductor (NASICON)-type materials ($Na_2FePO_4F$ and $NaFePO_4$) [13,14]).

However, the difference in size and electronegativity of Li and Na leads to fundamental distinctions in the chemistry of rechargeable lithium and sodium ion batteries. The effective ionic radius of $Na^+$ (102 pm) is larger than that of $Li^+$ (76 pm), therefore $Na^+$ tends to occupy octahedral and prismatic sites instead of tetrahedral sites. As a result, layer-structured $Na_xMO_2$ cathode materials with $Na^+$ occupying octahedral or prismatic sites are more stable and suitable compared with spinel $NaM_2O_4$ types with $Na^+$ at tetrahedral sites. Also, layer-structured cathodes deliver much higher capacities than other types of cathodes. The advantages of layer-structured cathodes have lent much momentum in this area of research in recent years. Two kinds of layered structures emerge in the mainstream, i.e. O- and P-types. In O-type cathodes such as $NaCrO_2$ [10] and $NaFeO_2$ [11], $Na^+$ takes octahedral sites. The structure of $Na_xMO_2$ with x close to 1 resembles that of $LiMO_2$ (R-3m). In P-type cathodes such as $Na_xCo_{1/3}Ni_{1/3}Mn_{1/3}O_2$, $Na^+$ occupies prismatic sites [12]. Prismatic sites between O-O layers pose less space constraints to $Na^+$ diffusion compared with octahedral sites, therefore, P-type cathodes often deliver higher reversible capacities and exhibit better rate performance and longer cycle life compared with O-type. However, $Na^+$ can only be partially taken out of P- type cathodes with typical x values in $Na_xMO_2$ between 0.5 and 0.8. Using sodium metal or sodium-reduced carbons as anodes, extra $Na^+$ intercalates into the P-type cathodes during the first discharge, which leads to higher capacities in subsequent cycles.

With sodium metal or sodium-reduced carbon as anodes, oxides ($VO_2$, $V_2O_5$) [15–18] and phosphates ($FePO_4$) [19] can also be employed as cathodes in secondary sodium ion batteries. The capacity of sodium ion batteries with oxides as cathodes can reach up to 300 mAh/g and the cycle performance is excellent with modifications using graphene quantum dots [15]. In particular materials containing transition metals with accessible high oxidation states such as Cr and V are desirable candidates for high-voltage cathodes. Electrochemically active chromium oxides

* Corresponding author at: Department of Chemistry and Biochemistry, Florida State University, Tallahassee, FL 32306, USA.
*E-mail address:* hu@chem.fsu.edu (Y.-Y. Hu).

http://dx.doi.org/10.1016/j.jssc.2016.05.004
0022-4596/

include $Cr_3O_8$, $Cr_8O_{21}$, and $Cr_2O_5$. When chromium oxides employed in rechargeable lithium ion batteries in our prior studies, the potential is 3.0 V *vs.* $Li/Li^+$ [20–23] with an energy density of more than 300 mAh/g [23]. For instance, $Cr_2O_5$ synthesized by pyrolysis of $CrO_3$ delivered a high specific energy of 330 mA/g and a power density of 819 Wh/kg. In addition to all the advantages mentioned above, Cr is more abundant with lower cost compared with common transition metals used in cathodes and the synthesis temperature of chromium oxides is much lower than other oxides [10–12]. In this work, we applied $Cr_2O_5$ as cathodes in rechargeable sodium ion batteries, which offered a power density of 541 Wh/kg upon discharge and 700 Wh/kg upon charge and a specific capacity up to 310 mAh/g. In conjunction to electrochemical measurements, the reaction mechanisms of the discharge-charge process have been investigated in details using advanced solid-state $^{23}Na$ projection-magic-angle-turning-phase-adjusted-spinning-sideband (pjMATPASS) NMR, powder X-ray diffraction (XRD) and thermal gravimetric analysis (TGA).

## 2. Experimental

### 2.1. Materials synthesis

Chromium oxide, $Cr_2O_5$, was synthesized by pyrolysing $CrO_3$ (Sigma Aldrich) at 350 °C for 10 h. When heated, $CrO_3$ melted and decomposed to form a brown bulk material, and then this bulk material was manually grounded using an agate mortar and pestle to a fine powder with an average particle size of several micrometers [23].

### 2.2. Materials characterization

Thermal gravimetric analysis (TGA) of $CrO_3$ was performed under air atmosphere (TA instrument, Q50) with a heating rate of 3 °C/min, up to 350 °C and the temperature was held at 350 °C for 20 h.

The chemical phase composition of these synthesized chromium oxides was determined by X-ray diffraction (XRD) (X'PERT Pro MPD, Cu Kα radiation, λ=0.15406 nm). The diffraction patterns were recorded at room temperature in the 2θ range from 10° to 40°. After electrochemical cycling, the coin cells were disassembled and washed with dimethyl carbonate (DMC) 3 times in an Ar-filled glovebox, and then the cycled electrodes were scraped off the aluminum current collector and grounded to fine powders for XRD and NMR characterization.

### 2.3. Fabrication of battery cells and electrochemical measurements

To make cathode films, $Cr_2O_5$, acetylene black, 5 wt% polyvinylidene fluoride (PVDF) dissolved in N-methyl-2-pyrrolidinone (NMP), and extra NMP, were mixed together to form a uniform slurry. The slurry was then casted on the carbon coated aluminum foil (current collector) and dried at 120 °C. The cathode film was composed of 70 wt% $Cr_2O_5$, 20 wt% acetylene black, and 10 wt% PVDF binder. The film was punched into discs with a diameter of 12.5 mm for fabricating coin-type cells. To prepare the sodium counter electrode, a block of sodium metal was cut into small ribbons and punched into discs with a diameter of 14 mm. The coin cells were assembled with glass microfiber filters (Whatman, GE healthcare) as the separator and 1 M $NaClO_4$ in propylene carbonate as the electrolyte in an argon-filled glovebox (MBraun).

The electrochemical performance of these $Cr_2O_5$/Na coin cells were examined using a multi-channel battery test system (Arbin) with an optimized potential window between 1.0 V and 4.0 V *vs.* $Na/Na^+$. The AC impedance and cyclic voltammetry (CV) of these batteries were measured at room temperature on a Reference 600 (Gamry Instruments), with a frequency range from 1 Hz to $10^5$ Hz and a voltage window from 1.0 V to 4.0 V with a scan rate of 0.2 mV/s.

### 2.4. NMR characterization

High-resolution $^{23}Na$ MAS NMR spectra of pristine and cycled chromium oxide electrodes were acquired at a Larmor frequency of 291.5 MHz on a Bruker Avance 830 MHz spectrometer with a home-built 1.8-mm MAS probe spinning at 25 kHz. Due to the extremely broad spectral range of paramagnetic $^{23}Na$ NMR resonance and overlapping spinning sidebands, 2D rotor-synchronized projection magic-angle turning phase-adjusted sideband separation (pjMATPASS) pulse sequence with 16 $t_1$ increments was employed for all measurements [24]. The solid 90° pulse length was 0.85 μs to ensure broadband excitation. The recycle delay was 0.1 s. $^{23}Na$ shifts were calibrated by using a 1 M NaCl solution (0 ppm).

## 3. Results and discussions

### 3.1. Thermal transformation of chromium oxides

The weight loss and phase transformation of $CrO_3$ during the pyrolysis process have been probed by TGA and powder XRD as

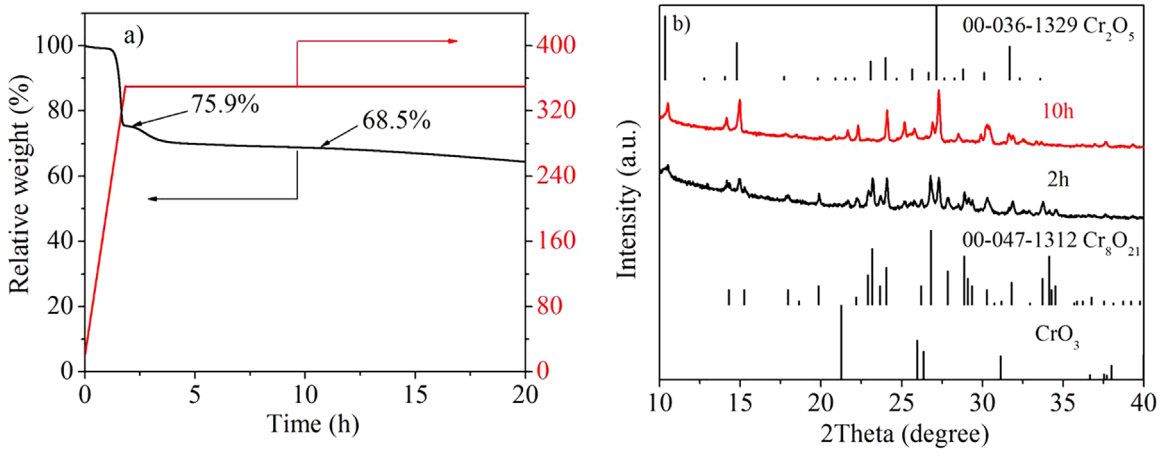


**Fig. 1.** (a) Thermal gravimetric analysis of $CrO_3$ heated to 350 °C for up to 20 h. b) Powder X-ray diffraction patterns of $CrO_3$ heated to 350 °C for 2 h and 10 h and the reference patterns of $CrO_3$, $Cr_8O_{21}$ and $Cr_2O_5$ phases. [26,27].

shown in Fig. 1. TGA results demonstrate that $CrO_3$ starts to decompose at around 300 °C, and the initial weight loss corresponding to the first decomposition process is 24% (Fig. 1a). The second-stage decomposition occurs at 350 °C accompanied by another 8% weight loss. Thermal decomposition of $CrO_3$ has been extensively studied before [25] and the decomposition products of these two decomposition processes were identified as $Cr_8O_{21}$ and $Cr_2O_5$. The weight loss from $CrO_3$ to $Cr_8O_{21}$ should be only 6% and from $Cr_8O_{21}$ to $Cr_2O_5$ 2%. The extra weight loss comes from the vaporization of $CrO_3$. Slight decrease in weight was observed even after 20-h heating, suggesting minor further decomposition or vaporization of remaining $CrO_3$.

Powder XRD was employed to assist with phase identification. XRD patterns of $CrO_3$ heated for 2 h and 10 h are shown in Fig. 1b together with the XRD patterns of $Cr_8O_{21}$ (00-047-1312 [26]) and $Cr_2O_5$ (00-036-1329 [27]) found in the crystallography database. The starting material $CrO_3$ (space group: *Ama*2, a=5.7430 Å, b=8.5570 Å and c=4.7890 Å) has a one-dimensional crystal structure formed by corner-linked $CrO_4$ tetrahedra. Upon heat treatment, $CrO_3$ first decomposes to triclinic $Cr_8O_{21}$ (*P*-1, a=5.4330 Å, b=6.5570 Å, c=12.1170 Å, α=106.3500°, β=95.7300°, γ=77.9600°), which contains chromium (III), chromate, and tetrachromate groups. The composition of $Cr_8O_{21}$ can be given as $Cr(III)(Cr(VI)O_4)_2(Cr(VI)_4O_{13}$. Further heated, $Cr_8O_{21}$ converts to monoclinic $Cr_2O_5$ (a=12.01 Å, b=8.52 Å, c=9.39 Å, β=92.0°) with a composition of $Cr(III)_2Cr(VI)_4O_{15}$. With continuous reduction/de-oxygenation, the Cr(III)/Cr(IV) increases from $CrO_3$ to $Cr_8O_{21}$ and eventually to $Cr_2O_5$. It is worth noting that when the 10-h sample was dispersed in distilled water, the filtered solution exhibited an orange color (Fig. S1), which is an indication of residual $CrO_3$. After several rounds of washing and filtering, the pure-phase $Cr_2O_5$ is obtained and used as a cathode material in rechargeable sodium ion batteries in this investigation.

### 3.2. Chromium oxides as cathodes in rechargeable sodium ion batteries

Chromium oxide, $Cr_2O_5$, exhibited higher specific capacities compared with most cathodes employed in rechargeable sodium ion batteries. When $Cr_2O_5$/Na cells discharged to 1.0 V (Fig. 2a), the $Cr_2O_5$ cathode delivered a specific capacity of ~270 mAh/g at a current density of 0.2 C (1 C=300 mA/g). When cycled at lower current density (e.g., 0.0625 C), the capacity of $Cr_2O_5$ increases to about 310 mAh/g (Fig. S2). The slow rate performance is a result of poor electronic conductivity of $Cr_2O_5$ and can be improved by increasing the content of conductive carbon matrix in the cathode. The discharge voltage of $Cr_2O_5$/Na cell is close to 2.0 V and thus the energy density can reach 541 Wh/kg. Cr(VI)/Cr(III) is the active redox couple. Upon Na intercalation into chromium oxides during discharge process, Cr(VI) is reduced to Cr(III); upon Na de-intercalation during charge process, Cr(III) is oxidized to Cr(VI). The first discharge and charge cycle yielded a coulombic efficiency of 91%.

Cyclic voltammetry (Fig. 2b) proffers a clearer account of the reduction potentials of relevant redox reactions involved in the electrochemical process. The $Cr_2O_5$/Na battery exhibited a broad redox peak with the center at 1.55 V during discharge, and no clear peak was observed during charge. The difference in the discharge and charge profiles resulted from significant structural change (amorphization) during the first discharge as evidenced from both XRD and NMR data discussed in the following.

### 3.3. Fate of $Na^+$ probed by solid-state $^{23}Na$ NMR

High-resolution solid-state $^{23}Na$ NMR was employed to track the fate of Na ions when the $Cr_2O_5$/Na batteries were cycled to different states of charge. The 2D pjMATPASS method [24] was applied to achieve high resolution. The details of the pjMATPASS data acquisition and processing are described in the experimental part and SI.

The high-resolution $^{23}Na$ NMR spectra of $Cr_2O_5$ electrodes at different states of charge are shown in Fig. 3a. At the early stage of discharge (2 V), three Na local environments are shown. The sharp NMR resonance around 0 ppm is the signature of Na ions in the solid-electrolyte-interphase (SEI), indicating that minor SEI forms even at the beginning of the discharge process. The remaining two NMR peaks are displaced far away from 0 ppm and this displacement is paramagnetic shift induced by the interaction between the Na nuclei and the unpaired electrons in $Cr^{3+}$. The two NMR peaks with large paramagnetic shifts are assigned to Na ions intercalated into the bulk $Cr_2O_5$ structure. The sharp peak at 380 ppm is from Na ions inserted in the crystalline-phase $Cr_2O_5$. This single peak with narrow linewidth indicates a homogeneous distribution of $Cr^{3+}$ and $Cr^{6+}$ within the bulk $Cr_2O_5$ structure. However, this sharp resonance is short-lived as the discharge process proceeds further. It converts to the broad resonance underneath it as the continuous intercalation of Na ions turns the crystalline $Cr_2O_5$ to a disordered structure. The sharp resonance disappears completely in electrodes discharged below 1.8 V, with the broad component dominants the spectra at low voltages. Below 1.8 V, a dramatic increase in fraction of the diamagnetic component at 0 ppm is observed, indicating a significant amount of SEI formation at low voltages, while the amount of Na ions in the bulk remains nearly constant. Upon charge, Na ions are first stripped out of the SEI

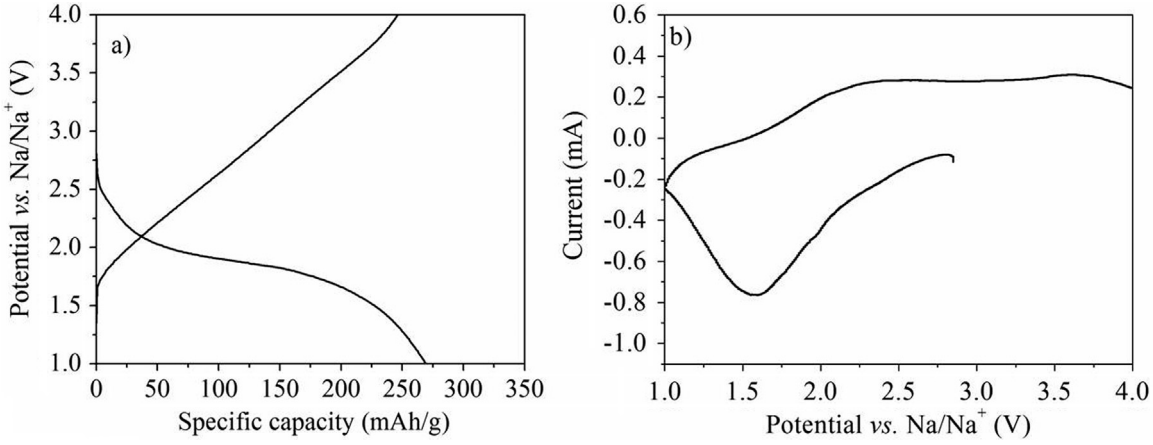


**Fig. 2.** (a) The first-cycle charge-discharge profile and b) the cyclic-voltammetry of $Cr_2O_5$/Na batteries.

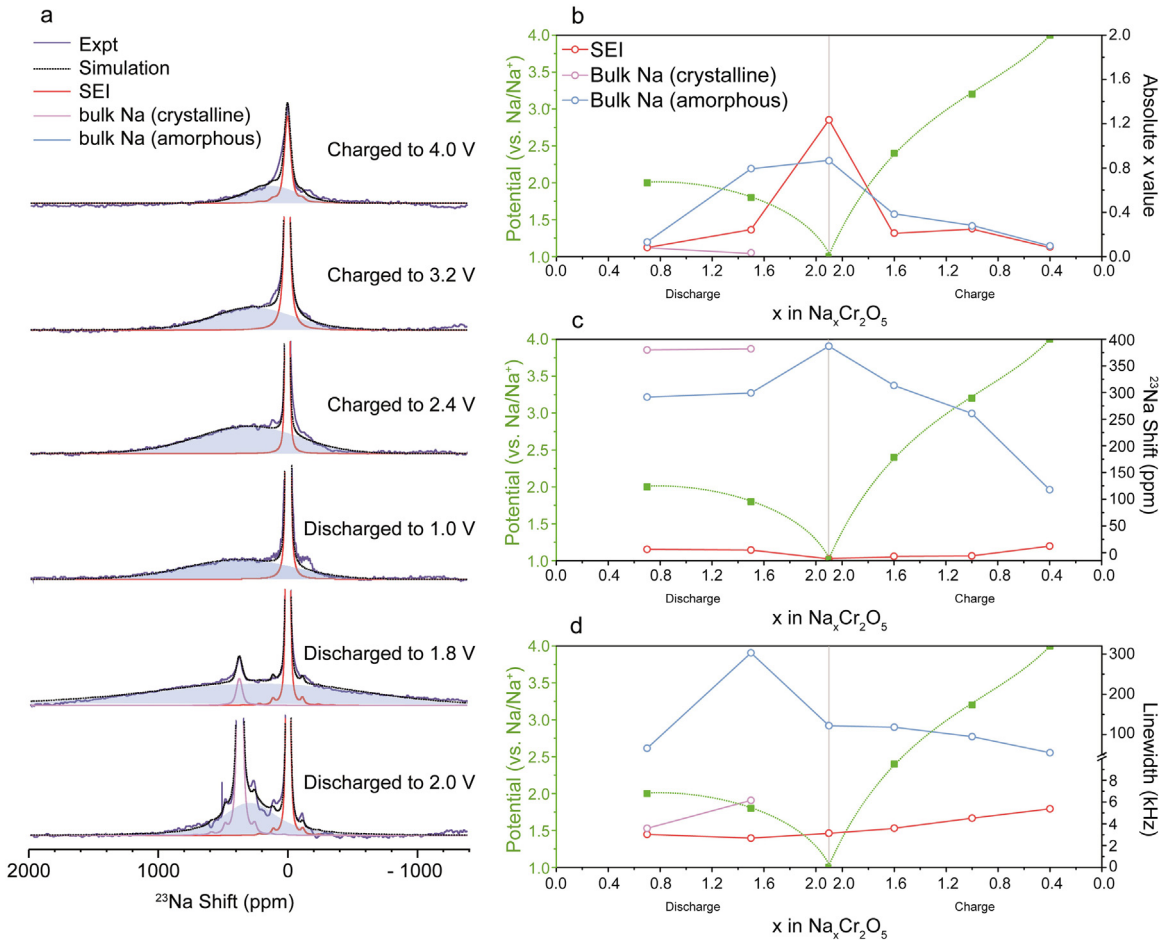


**Fig. 3.** (a) High-resolution solid-state $^{23}$Na MAS NMR spectra of $Cr_2O_5$ electrodes at different states of charge (the top of the $^{23}$Na resonance at 0 ppm is omitted in order to more clearly show the broad $^{23}$Na resonance. The un-edited series of $^{23}$Na spectra can be found in the SI) b) quantification of 3 major Na-containing species formed in the $Cr_2O_5$ cathodes during battery cycling, c) the evolution of the $^{23}$Na shifts, and d) linewidth of the $^{23}$Na resonances during the first discharge and charge cycle.

layer, and gradual extraction of Na from the disordered bulk is observed through the whole charge process. The broad Na resonance shifts towards 0 ppm as $Cr^{3+}$ is oxidized to $Cr^{6+}$ with Na extraction. Minor Na remains in both the SEI and bulk even at the top of charge (4.0 V). The quantification plot of each Na resonance through the first discharge-charge cycle is shown in Fig. 3b. Based on the quantification, it is estimated that one unit of Na per $Cr_2O_5$ is intercalated into the bulk, which makes it $NaCr_2O_5$. The nominal composition $NaCr_2O_5$ indicates that the Cr(III)/Cr(IV) is increased to 1 at the end of discharge from the 1/2 in pristine $Cr_2O_5$. The detailed quantification of the three Na components also suggests that ~50% of Na does not intercalated into the bulk but forms Na-containing compounds in the SEI.

The evolution of the paramagnetic shifts (Fig. 3c) and linewidth (Fig. 3d) probes the changes in the $Na^+$ local structural environments in the $Cr_2O_5$ electrode at different states of charge. The increase in the paramagnetic shift of Na ions in the bulk electrode during discharge suggests stronger paramagnetic interactions between intercalated Na ions and unpaired electrons in $Cr^{3+}$, which is resulted from the increased amount of $Cr^{3+}$ in the bulk as $Cr^{6+}$ is reduced to $Cr^{3+}$ during discharge. The continuous decrease in paramagnetic shift of bulk Na ions is observed upon charge, indicative of the reduced amount of $Cr^{3+}$ by oxidation to $Cr^{6+}$. The $^{23}$Na paramagnetic shift of the residual bulk Na at the top of charge is much smaller than that of Na ions intercalated at the beginning of discharge. The smaller paramagnetic shift suggests a $Cr^{6+}$-rich environment at the top of charge, which may pose large overpotential for extracting $e^-$ out, accompanying $Na^+$ removal. The lack of significant change in the paramagnetic shift of the bulk Na in the crystalline $Cr_2O_5$ indicates a two-phase reaction at the early stage of discharge, i.e. the conversion of the crystalline to the amorphous $Cr_2O_5$ as more Na is intercalated. The chemical shift of the diamagnetic Na component in the SEI does not vary much.

The linewidth of the $^{23}$Na resonances depends on two factors, i.e., structural disorder and relaxation induced by paramagnetic interactions. As the discharge occurs, the structure becomes increasingly disordered and more $Cr^{6+}$ is reduced to $Cr^{3+}$ leading to stronger paramagnetic interactions thus fast relaxation, therefore, these two factors contribute constructively to broaden the Na resonance in the bulk electrode upon discharge. At the end of discharge, the structure becomes completely disordered, so the degree of structural disorder does not vary much, therefore, the relaxation mechanism determines the linewidth upon charge. As the $Cr^{3+}$ is oxidized to $Cr^{6+}$ during charge, the paramagnetic effects on $^{23}$Na decrease, which leads to slower relaxation and narrower linewidth. The linewidth of the bulk $^{23}$Na resonance does decrease upon charge as expected and increases at the beginning of discharge. The unexpected decrease in linewidth near the end of discharge is likely due to the loss of Na in the $Cr^{3+}$-rich phase due to extremely fast relaxation, and the remaining Na are from a $Cr^{3+}$ difficient phase with slower relaxation. The linewidth of the diamagnetic Na increases slightly over both discharge and charge due to structural disorder.

In summary, high-resolution $^{23}$Na NMR reveals that 50% of Na intercalates into the bulk $Cr_2O_5$ electrode with the rest forming diamagnetic Na-containing compounds in the SEI. The redox

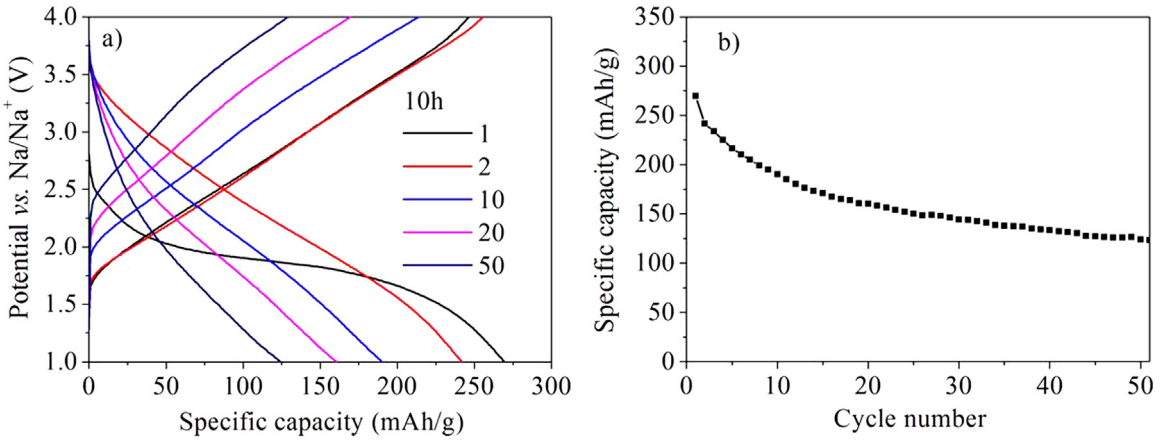


**Fig. 4.** Long-term cycling performance of the $Cr_2O_5$/Na cells. a) Selective electrochemical profiles of a $Cr_2O_5$/Na battery cell up to 50 cycles, b) specific capacities of chromium oxides/Na batteries recorded up to 50 cycles.

reaction between $Cr^{3+}$ and $Cr^{6+}$ during discharge and charge is reflected by the changes in paramagnetic shifts and linewidth of bulk Na resonance. The structural disorder induced by Na insertion into the bulk is observed through the two-phase conversion of the Na in the crystalline phase to Na in the amorphous phase at early stage of discharge.

### 3.4. Long-term cyclability

The long-term cyclability of $Cr_2O_5$/Na batteries was investigated and the results are shown in Fig. 4. Gradual capacity fading was observed at the beginning and the capacity was stabilized at 120 mAh/g over long-term cycling, which is comparable to most state-of-the-art Na ion battery systems.

The cause of the capacity fading was investigated with electrochemical impedance spectroscopy (EIS), solid-state $^{23}$Na NMR, and power X-ray diffraction (Fig. 5). Impedance spectroscopy of batteries after 1, 10, and 50 cycles (Fig. 5a) suggests increased internal charge transfer resistance (high-frequency region) and slower Na ion diffusion kinetics (low frequency Warburg region) as increasing the cycle numbers. The greater charge transfer resistance is likely due to the loss of electric contact among chromium oxide particles in the electrode as they were broken down with extended cycling. Slower $Na^+$ ion diffusion may be a result of reduced electrolyte concentration, as the electrolyte decomposition occurs to form solid electrolyte interphase (SEI), which in turn blocks $Na^+$ pathway. The results from detailed analysis of the EIS spectra are summarized in Table S1. Solid-state $^{23}$Na NMR of $Cr_2O_5$ cathodes at the top of charge after 50 cycles was acquired (Fig. 5b) and compared with that after 1 cycle, which showed significant residual Na built up within the SEI layer over multiple cycles. The continuously thickening SEI layer inevitably blocks Na transfer into the bulk and increases the impedance. The powder X-ray diffraction patterns of the $Cr_2O_5$ electrode at different states of charge during the first cycle and at the top of charge after 50 cycles are shown in Fig. 5c. Consistent with $^{23}$Na NMR results, structural amorphization occurs at very early stage of first discharge and the structure becomes completely amorphous at the end of first discharge. In the XRD pattern of the $Cr_2O_5$ electrode after 50 cycles, two major diffraction peaks at 2theta values near 22° and 26° are observed accompanied by other minor components, which are identified as crystalline $CrO_3$. It is likely that the formation of crystalline $CrO_3$ gradually builds up over multiple cycles. The aqueous washing solution of the cycled electrodes exhibited an orange color (Fig. S3), which is a typical signature of $CrO_3$ solution. As is known that $CrO_3$ is a powerful oxidizer [28] and may catalyze the decomposition of electrolytes. Electrolyte decomposition was indeed observed with $^1$H and $^{13}$C solid-state MAS NMR (Fig. S5).

Based on all the experimental evidence, the capacity fading in the $Cr_2O_5$/Na batteries may be caused by the following factors: 1) loss of electric contact resulting from particle break-down; 2) generation of strong oxidizing $CrO_3$, which leads to catalytic electrolyte decomposition and thick SEI formation that depletes Na electrolyte as well as blocks Na intercalation.

Further improvement in the electrochemical performance of $Cr_2O_5$-based rechargeable Na ion batteries can be made by stabilizing chromium oxide electrodes and preventing loss in electric conductivity with proper polymer binders or new morphologies of chromium oxides particles that is resistant to changes in structure. Surface modification can minimize the contact of chromium oxides surface and electrolyte and mitigate the issue of catalyzed electrolyte decomposition.

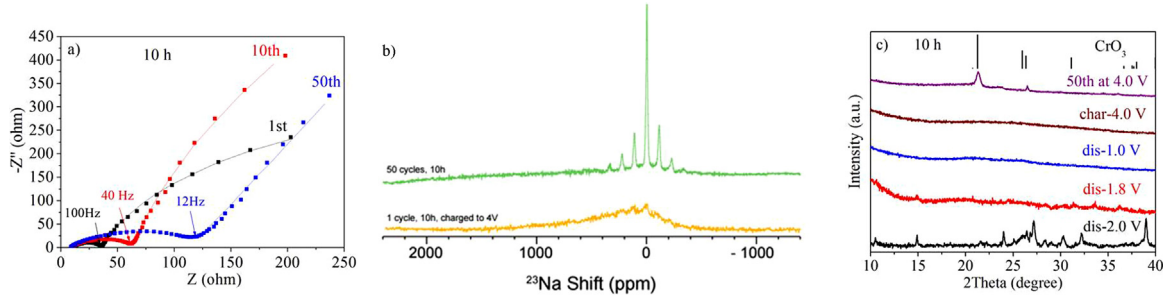


**Fig. 5.** Experimental evidence revealing the potential cause of capacity degradation, a) AC impedance spectroscopy of a $Cr_2O_5$/Na cell after 1, 10, and 50 cycles, b) solid-state $^{23}$Na MAS NMR of the chromium oxides electrode after 1 cycle and 50 cycles at the top of charge, c) powder XRD patterns of cycled $Cr_2O_5$ electrodes at different states of charge during the 1st cycle and at the top of charge after 50 discharge-charge cycles.

## 4. Conclusions

A new cathode material ($Cr_2O_5$) for rechargeable sodium ion batteries has been synthesized by pyrolysing $CrO_3$. The $Cr_2O_5$ electrode employs the $Cr^{6+}/Cr^{3+}$ redox couple and provides very high capacity of up to 310 mAh/g at a current density of C/16. The Na intercalation process was probed with high-resolution solid-state $^{23}$Na NMR, which has revealed that $>50\%$ of Na ions inserts into the bulk electrode and are adjacent to paramagnetic $Cr^{3+}$ with the remaining Na ion in the SEI. Na can be reversibly inserted and extracted through discharge and charge of the battery cells. However, minor Na remains in the bulk structure and SEI after each cycle, which leads to gradual capacity fading. For long-term cycling of the batteries, the energy capacity stabilizes at $>120$ mAh/g. Impedance spectroscopy, $^{23}$Na NMR, and powder-XRD data on cycled batteries have suggested that loss of electric contact due to structural amorphization and $CrO_3$-catalyzed electrolyte decomposition are among the major reasons for gradual capacity degradation. Mitigating strategies including incorporating proper polymer binders, surface modification, and new morphology design are being explored to improve the electrochemical performance of these high-energy-density electrodes for rechargeable sodium ion batteries.

## Acknowledgement

This study was supported by Florida State University. Work performed at the National High Magnetic Field Laboratory was supported by NSF Grant DMR-1157490 and the State of Florida.

## Appendix A. Supplementary material

Supplementary data associated with this article can be found in the online version at http://dx.doi.org/10.1016/j.jssc.2016.05.004.

## References

[1] F.Y. Cheng, J. Liang, Z.L. Tao, J. Chen, Adv. Mater. 23 (2011) 1695–1715.
[2] V. Palomares, P. Serras, I. Villaluenga, K.B. Hueso, J. Carretero-Gonzalez, T. Rojo, Energy Environ. Sci. 5 (2012) 5884–5901.
[3] M.D. Slater, D. Kim, E. Lee, C.S. Johnson, Adv. Funct. Mater. 23 (2013) 947–958.
[4] Y.L. Cao, L.F. Xiao, M.L. Sushko, W. Wang, B. Schwenzer, J. Xiao, Z.M. Nie, L. V. Saraf, Z.G. Yang, J. Liu, Nano Lett. 12 (2012) 3783–3787.
[5] Z.H. Wang, L. Qie, L.X. Yuan, W.X. Zhang, X.L. Hu, Y.H. Huang, Carbon 55 (2013) 328–334.
[6] Y.C. Liu, N. Zhang, L.F. Jiao, J. Chen, Adv. Mater. 27 (2015) 6702–6707.
[7] C. Yue, Y.J. Yu, S.B. Sun, X. He, B.B. Chen, W. Lin, B.B. Xu, M.S. Zheng, S.T. Wu, J. Li, J.Y. Kang, L.W. Lin, Adv. Funct. Mater. 25 (2015) 1386–1392.
[8] L.Y. Yang, H.Z. Li, J. Liu, S.S. Tang, Y.K. Lu, S.T. Li, J. Min, N. Yan, M. Lei, J. Mater. Chem. A 3 (2015) 24446–24452.
[9] Y. Sun, L. Zhao, H.L. Pan, X. Lu, L. Gu, Y.S. Hu, H. Li, M. Armand, Y.C. Ikuhara, L. Q. Chen, X.J. Huang, Nat. Commun. 4 (2013) 1870–1879.
[10] K. Kubota, I. Ikeuchi, T. Nakayama, C. Takei, N. Yabuuchi, H. Shiiba, M. Nakayama, S. Komaba, J. Phys. Chem. C 119 (2015) 166–175.
[11] N. Yabuuchi, H. Yoshida, S. Komaba, Electrochemistry 80 (2012) 716–719.
[12] M. Sathiya, K. Hemalatha, K. Ramesha, J.M. Tarascon, A.S. Prakash, Chem. Mater. 24 (2012) 1846–1853.
[13] R. Tripathi, S.M. Wood, M.S. Islam, L.F. Nazar, Energy Environ. Sci. 6 (2013) 2257–2264.
[14] N. Wongittharom, T.C. Lee, C.H. Wang, Y.C. Wang, J.K. Chang, J. Mater. Chem. A 2 (2014) 5655–5661.
[15] D.L. Chao, C.R. Zhu, X.H. Xia, J.L. Liu, X. Zhang, J. Wang, P. Liang, J.Y. Lin, H. Zhang, Z.X. Shen, H.J. Fan, Nano Lett. 15 (2015) 565–573.
[16] W. Wang, B. Jiang, L.W. Hu, Z.S. Lin, J.G. Hou, S.Q. Jiao, J. Power Sources 250 (2014) 181–187.
[17] H.Y. Li, C.H. Yang, C.M. Tseng, S.W. Lee, C.C. Yang, T.Y. Wu, J.K. Chang, J. Power Sources 285 (2015) 418–424.
[18] D.W. Su, G.X. Wang, ACS Nano 7 (2013) 11218–11226.
[19] W. Wang, S.B. Wang, H.D. Jiao, P. Zhan, S.Q. Jiao, Phys. Chem. Chem. Phys. 17 (2015) 4551–4557.
[20] J.Y. Liu, Z.X. Wang, H. Li, X.J. Huang, Solid State Ion. 177 (2006) 2675–2678.
[21] R. Vidya, P. Ravindran, A. Kjekshus, H. Fjellvag, Phys. Rev. B 73 (2006) 235113.
[22] R.P. Ramasamy, B. Veeraraghavan, B. Haran, B.N. Popov, J. Power Sources 124 (2003) 155–162.
[23] X.Y. Feng, N. Ding, L. Wang, X.H. Ma, Y.M. Li, C.H. Chen, J. Power Sources 222 (2013) 184–187.
[24] I. Hung, L. Zhou, F. Pourpoint, C.P. Grey, Z.H. Gan, J. Am. Chem. Soc. 134 (2012) 1898–1901.
[25] S.A.A. Sajadi, M. Khaleghian, J. Therm. Anal. Calorim. 116 (2014) 915–921.
[26] P. Norby, A.N. Christensen, H. Fjellvag, M. Nielsen, J. Solid State Chem. 94 (1991) 281–293.
[27] T.A. Hewston, B.L. Chamberland, J. Magn. Magn. Mater. 43 (1984) 89–95.
[28] P.M.C. Zapataa, M.S. Nazzarrob, E.E. Gonzoc, M.L. Parentisc, N.A. Boninia, Catal. Today 259 (2015) 39–49.